

Carrier leakage into the continuum in diagonal GaAs/Al_{0.15}GaAs terahertz quantum cascade lasers

Asaf Albo and Qing Hu

Citation: [Applied Physics Letters](#) **107**, 241101 (2015); doi: 10.1063/1.4937455

View online: <http://dx.doi.org/10.1063/1.4937455>

View Table of Contents: <http://scitation.aip.org/content/aip/journal/apl/107/24?ver=pdfcov>

Published by the [AIP Publishing](#)

Articles you may be interested in

[λ ~ 3.1 μ m room temperature InGaAs/AlAsSb/InP quantum cascade lasers](#)

Appl. Phys. Lett. **94**, 031106 (2009); 10.1063/1.3073865

[Experimental investigation of the lattice and electronic temperatures in Ga_{0.47}In_{0.53}As/Al_{0.62}Ga_{0.38}As_{1-x}Sb_x quantum-cascade lasers](#)

Appl. Phys. Lett. **90**, 121109 (2007); 10.1063/1.2717018

[Doping in quantum cascade lasers. II. GaAs/Al_{0.15}Ga_{0.85}As terahertz devices](#)

J. Appl. Phys. **100**, 043102 (2006); 10.1063/1.2234805

[Above room temperature operation of short wavelength \(λ = 3.8 μ m\) strain-compensated In_{0.73}Ga_{0.27}As – AlAs quantum-cascade lasers](#)

Appl. Phys. Lett. **85**, 1478 (2004); 10.1063/1.1789246

[Lasing properties of GaAs/\(Al,Ga\)As quantum-cascade lasers as a function of injector doping density](#)

Appl. Phys. Lett. **82**, 671 (2003); 10.1063/1.1541099

The advertisement for MMR Technologies features a blue and white background with a grid pattern. On the left is the MMR Technologies logo, which consists of a stylized 'M' and 'R' in a blue and red arc, with 'TECHNOLOGIES' written below. To the right of the logo is the text 'THE WORLD'S RESOURCE FOR VARIABLE TEMPERATURE SOLID STATE CHARACTERIZATION' in bold, black, uppercase letters. Below this text are five images of different scientific instruments: an optical study system, a Seebeck study system (SB1000 and K2000), a microprobe station, a Hall effect study system (MS000 and K2000), and a magnet assembly. At the bottom left, the website 'WWW.MMR-TECH.COM' is displayed in red. Below each image is a label: 'OPTICAL STUDIES SYSTEMS', 'SEEBECK STUDIES SYSTEMS', 'MICROPROBE STATIONS', and 'HALL EFFECT STUDY SYSTEMS AND MAGNETS'.

Carrier leakage into the continuum in diagonal GaAs/Al_{0.15}GaAs terahertz quantum cascade lasers

Asaf Albo^{a)} and Qing Hu

Department of Electrical Engineering and Computer Science and Research Laboratory of Electronics, Massachusetts Institute of Technology, Cambridge, Massachusetts 02139, USA

(Received 26 October 2015; accepted 23 November 2015; published online 14 December 2015)

The maximum operating temperature reported so far for THz-QCLs is ~ 200 K. With the well-known degradation mechanism of thermally activated LO-phonon scattering, one straightforward strategy to improve their temperature performances is the use of diagonal structures in which the upper-to-lower state scattering time is lengthened. However, the effectiveness of this method for achieving room temperature operation remains to be demonstrated. Here, we studied the temperature degradation of highly diagonal GaAs/Al_{0.15}GaAs THz-QCLs. By analyzing their output power dependence on temperature, we identified the physical mechanism that limits their performance to be thermally activated leakage into the continuum, as evidenced by the large activation energy of ~ 80 meV extracted from the Arrhenius plot. This observation is further supported by a careful analysis of current-voltage characteristics, especially in regions of high biases. In order to significantly improve the temperature performances of diagonal THz-QCLs, this leakage should be eliminated. © 2015 AIP Publishing LLC. [<http://dx.doi.org/10.1063/1.4937455>]

The maximum operating temperature (T_{\max}) reported so far for a pulsed operation of terahertz quantum cascade lasers (THz-QCLs) is ~ 200 K.¹ For THz-QCLs based on spatially vertical transitions, the major physical mechanism that limits T_{\max} and reduces the population inversion at elevated temperatures is thermally activated LO-phonon scattering from the upper-to-lower lasing level.² Therefore, one straightforward strategy for overcoming the temperature degradation of THz-QCLs is by reducing the thermally activated LO-phonon scattering rate by using highly diagonal structures³ (see Figure 1). However, the effectiveness of this method for achieving significantly higher T_{\max} values than ~ 200 K remains to be demonstrated. The reason for the lack of improvement is unclear, and till date, the limiting mechanism has not been identified. Here, we studied the temperature degradation of GaAs/Al_{0.15}GaAs-based highly diagonal THz-QCLs and identified the mechanism that limits their performance.

The theoretically expected behavior of the output power dependence on temperature for different oscillator strength values is simulated in Figure 1. The simulation was conducted similarly to that presented in Ref. 2. The only temperature dependent mechanism that was included for this calculation is the thermally activated LO-phonon scattering between the upper and lower lasing states. The activation energy barrier, $E_a = E_{LO} - h\nu$, is the same for similar lasing energies. It is clear from the theoretical results that when the oscillator strength between these states is reduced, which corresponds to a greater spatial separation of the upper- and lower-state wavefunctions, the normalized output power versus temperature yields higher relative values at elevated temperatures. Since the emission power is proportional to the unclamped population inversion,² this slower temperature degradation for diagonal structures should result in a higher T_{\max} . Clearly, this

behavior is due to a higher raw LO-phonon scattering time, τ_{LO} , and consequently longer thermally activated LO-phonon scattering time, $\tau_{ul} = \tau_{LO} \times e^{\frac{E_{LO}-h\nu}{kT}}$, where, E_{LO} is the LO-phonon energy, $h\nu$ is the photon energy, and kT is the thermal energy (k is the Boltzmann constant and T is the temperature). Accordingly, when the oscillator strength is reduced from $f=1$ to $f=0.2$, the T_{\max} is supposed to increase significantly.

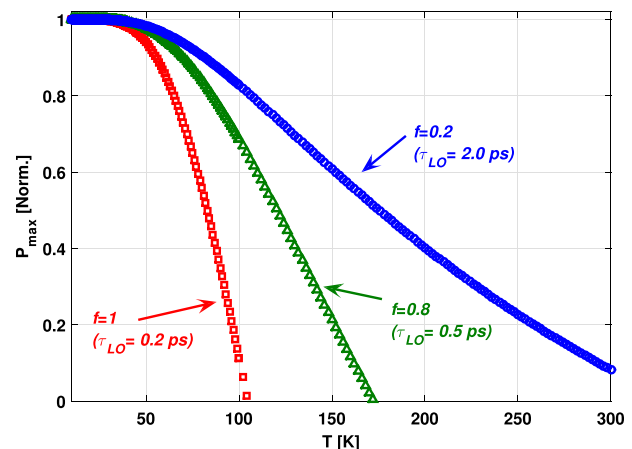


FIG. 1. Simulated normalized output power versus temperature curves with reduced oscillator strength: $f=1.0, 0.8, 0.2$. The only temperature dependent mechanism that was included in the calculations is the thermally activated LO-phonon scattering from the upper-to-lower lasing state. The activation energy barrier, $E_a = E_{LO} - h\nu$, is the same (for similar lasing energies) for all the structures. The oscillator strength is a measure of the degree of diagonality in lasing transition, where lower values indicate higher diagonality, i.e., lower wavefunctions overlap between the upper and lower lasing states. Due to the increase in the raw LO-phonon scattering time, τ_{LO} , with reducing the oscillator strength and the consequent increase of the thermally activated upper-to-lower state scattering time $\tau_{ul} = \tau_{LO} \times e^{\frac{E_{LO}-h\nu}{kT}}$, the normalized output power show higher relative values. This slower temperature degradation for the diagonal structure should lead to a significantly increased T_{\max} .

^{a)}asafalbo@gmail.com

TABLE I. The device data. Additional details can be found in Refs. 8 and 9.

Device	Design name (wafer number)	Lasing energy (meV)	Oscillator strength	Expected activation energy (meV)	Layer sequence [#ML], and doping level	Process details ^a
LBV	FL183R-2 (EA1229)	19	1	17	17/29/6/24/14/58/12/32 $1.9 \times 10^{16} \text{ cm}^{-3}$ in 58 ML well	MM (Ta/Cu) Wet etched
LBD	OWI210H-M3 (VB0605)	16	0.2	20	19.8/29.5/12.8/30.5/16.6/57.6 $1.24 \times 10^{17} \text{ cm}^{-3}$ in the centered 17 ML of the 57.6 ML well	MM (Ta/Au) Dry etched

^aIn the process details column: the MM stands for metal-metal waveguide, where in the flowing brackets are the metal sequence used. In the lower line, the type of etching method used in the process is mentioned. In the layer sequence column, the #ML stand for number of monolayers, the bold values in the sequence indicate barrier layers, the doped layer in the sequence is underscored, and the doping details are elaborated in the following line. Additional details on the process can be found in Refs. 8 and 9.

For this study, we focused on a highly diagonal THz-QCL with an oscillator strength of $f \sim 0.2$ (device LBD, design OWI210H-M3 and MBE wafer VB0605) and compared it with a reference QCL (device LBV, design FL183R-2 and MBE wafer EA1229) with a typical vertical structure and an oscillator strength of $f \sim 1.0$. As a result of the increased diagonality in device LBD, the calculated τ_{LO} was increased to ~ 1.7 ps (as compared to ~ 0.25 ps for device LBV) and the upper-to-lower state LO-phonon scattering time will be always longer than 2 ps at elevated temperatures, which compares favorably to the ~ 0.5 -ps extraction time from the lower state. The notations “D” and “V” in the devices’ name stand for “Diagonal” and “Vertical” designs, respectively, and the notation “LB” stands for “low barriers,” i.e., barriers with the standard composition of 15% aluminum. A list of devices, summarizing the details of layer sequences and parameters, is presented in Table I. We would like to emphasize that device LBD was doped only at the centered 17 monolayers (ML) of its wider well (the injector well) in order to minimize any possible temperature

dependent effects that may result from the dopant impurities (as, for example, tunneling through impurities).

The band structure, pulsed light-current (L-I) measurements, and lasing spectra of devices LBV and LBD are shown in Figures 2(a), 2(b) and 2(c), 2(d), respectively. These devices have similar lasing frequencies around ~ 4 THz and both exhibit approximately the same T_{\max} value. As evidenced from the experimental data, unlike the theoretical expectations (Figure 1), T_{\max} did not improve significantly upon reducing the oscillator strength from $f \approx 1.0$ to 0.2. Furthermore, there is a major difference between the two devices regarding the deterioration rate of the output power with increased temperatures. Whereas the maximum output intensity of device LBV starts to decrease at low temperatures (see the difference between the 6 and 100 K measurements in Figure 2(a)), the maximum output intensity of device LBD remains nearly constant in this range (see the measurements at 11 and 112 K in Figure 2(c)), and at higher temperatures it drops sharply. This distinctive difference suggests a different thermal degradation mechanism in

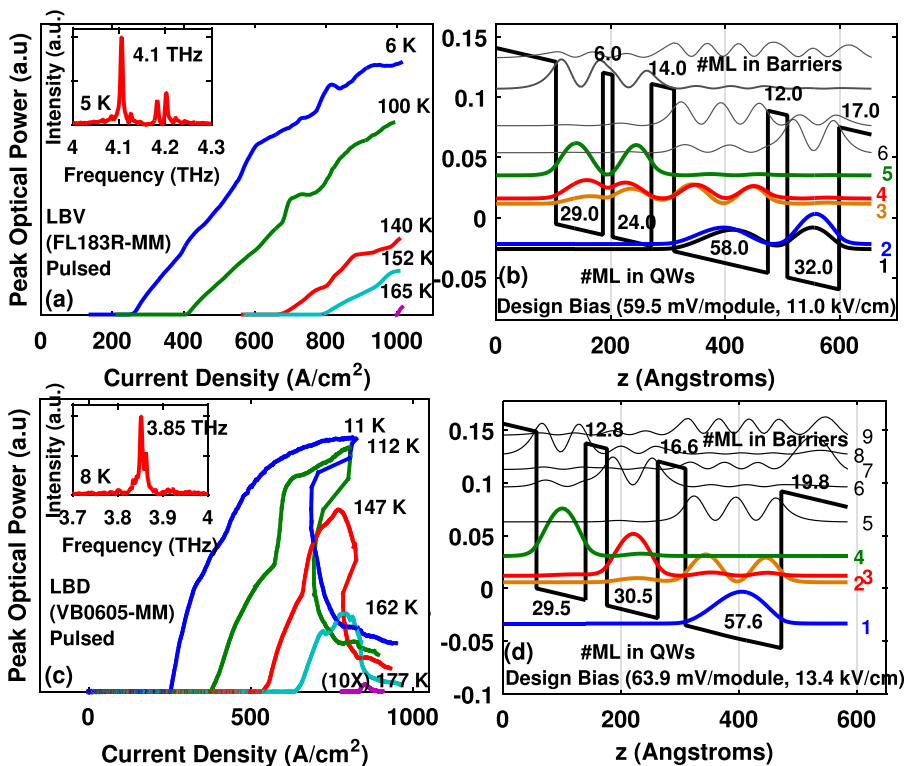


FIG. 2. (a) Pulsed light-current measurements for device LBV (FL183R2-MM), its lasing spectra (inset), and (b) its band diagram. (c) Pulsed light-current measurements for device LBD (VB0605-MM), its lasing spectra (inset), and (d) its band diagram.

highly diagonal structures. To study it, we analyzed in-depth the output power dependence on temperature, based on the method in Ref. 2.

The normalized maximum output power dependence on temperature is presented in Figure 3(a). The previously described observation is clearer from this figure. The output power of device LBV starts to decrease at low temperatures around 40 K and deteriorates at a relatively moderate rate, as predicted by the thermally activated LO-phonon relaxation mechanism.² In clear contrast, the output intensity of device LBD generally remains constant up to ~ 120 K, but above that value, it drops very sharply.

To identify the physical mechanisms underlying this behavior, we extracted the activation energies from the Arrhenius plots according to $\ln(1 - \frac{P_{out}(T)}{P_{outmax}}) \approx \ln(a) - \frac{E_a}{kT}$ as performed in Ref. 2, where P_{out} is the output power and a is a constant. We argue that this method is still valid for device LBD even though it shows a saturation in its low temperature L-I curves which are highly nonlinear (sublinear), Figure 2(c). We postulate our argument on the validity of the output power being proportional to the stimulated emission rate, which holds even in the general case of non-linear L-I: $P_{out} \sim (J - J_{th}(J) - \Delta J_L(J)) \sim \frac{1}{\tau_{st}}$, where $J_{th}(J)$ and $\Delta J_L(J)$ are the current-dependent threshold and leakage currents, respectively.⁴ So, as long as a clear exponential decrease of the output power with temperature increase is experimentally observed at a constant current, it should be directly related to a microscopic mechanism that governs the deterioration of the stimulated emission rate.

The experimental curves and activation energies are presented in Figure 3(b). The exponential behavior of the normalized power drop is clearly seen over a two-decade span, especially for the highly diagonal LBD device, thus validating the activation energy model used in our analysis. A clear difference was observed between devices LBV and LBD.

The activation energy of device LBD, ~ 80 meV, is much higher than the value expected from thermally activated LO-phonon relaxation and is also much higher than the injector to extractor separation of ~ 36 meV, which suggests that neither thermally activated LO-phonon scattering nor thermal backfilling is the likely culprit of the temperature degradation. In contrast, the activation energy value of device LBV, ~ 20 meV, is in close agreement with the one predicted by using its measured lasing frequency, indicating thermally activated LO-phonon relaxation.²

The activation energy value of device LBD suggests that thermal excitation of carriers occurs for states located energetically around the barriers' heights. Such resonances undergo very strong interactions with the continuum and thus have significant broadening,^{5,6} which results in a very fast escape rate into the continuum. Consequently, once this leakage channel becomes energetically allowed at high temperatures, the deterioration will be very fast. In contrast, in a vertical structure, the fast thermally activated LO-phonon scattering (with a sub-picosecond time scale at elevated temperatures) starts to dominate the degradation at lower temperature, and it likely masks this leakage channel to the continuum at temperatures below T_{max} . Accordingly, based on the above experimental results, our interpretation is that the main limiting mechanism for device LBD (in terms of temperature performance) is the thermally activated escape of the confined carriers into the continuum.

To further examine our interpretation, we investigated the behavior of the threshold current and the current-voltage (I-V) curves of both devices. Figure 3(c) shows the threshold current density, J_{th} , dependence on temperature. For the vertical structure LBV, J_{th} rises exponentially at high temperature and its behavior can be well characterized by the standard model of $J_{th}(T) = J_o e^{T/T_o}$ with $T_o \approx 73$ K. For the highly diagonal structure LBD, however, the exponential

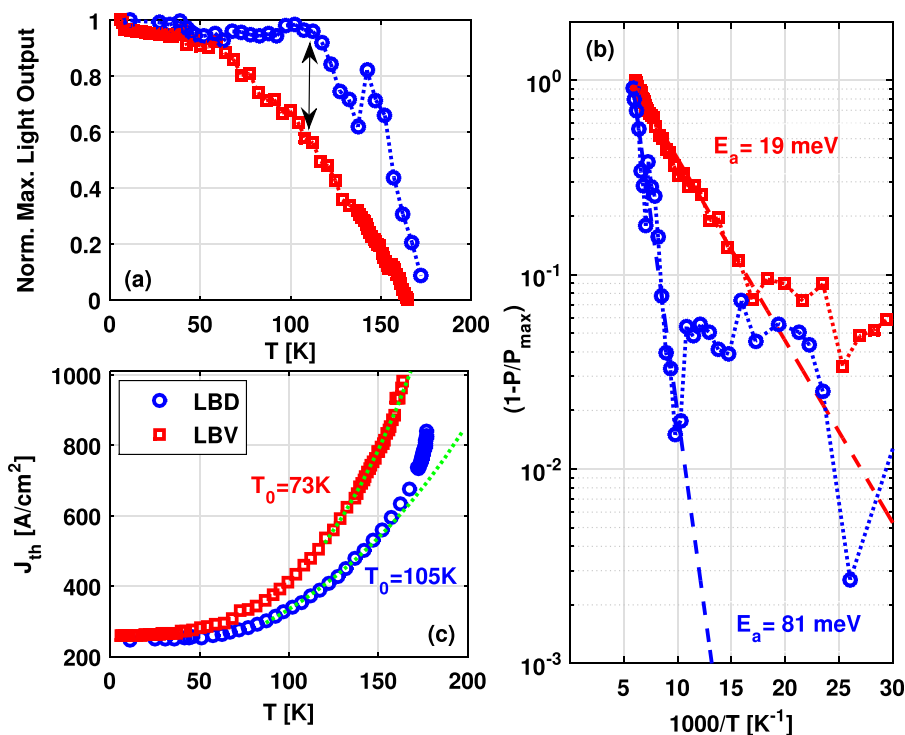


FIG. 3. (a) Normalized output light intensity versus temperature and (b) semi-logarithmic plots of $(1 - \frac{P_{out}(T)}{P_{outmax}})$ with fittings (dashed lines) and activation energy values. (c) Threshold current densities versus temperature with T_0 values (and data marked for extraction with extrapolation). The data are denoted by red squares for device LBV and by blue circles for device LBD.

behavior only occurs at temperatures not too close to T_{max} , with a more favorable $T_o \approx 105$ K, whereas at temperatures near T_{max} , a super-exponential rise is observed and J_{th} rises sharply. This super-exponential rise in the threshold current indicates the onset of a new mechanism that affects the lasing process especially at high temperatures. This mechanism is likely the leakage to continuum. The reasoning behind this interpretation is that due to the high velocity of electrons in the continuum any small increase in the carrier concentration there results in highly intensified (parallel leakage) current that increases sharply with temperature, as experimentally observed.

The I-V curves of device LBD, measured at several temperatures (Figure 4), show typical I-V characteristics for resonant-phonon THz-QCL structures with a pronounced negative differential resistance (NDR) region at low temperatures (see, for example, the I-V curve taken at 11 K). The NDR occurs when the preceding module injector level 1' (not shown in Fig. 2(d)) is raised above the upper lasing level 4. Beyond the NDR region, the current increases again with the bias voltage resulting in a change to positive conductance. A careful analysis of the temperature dependence of the NDR region is informative. The onset voltage of the NDR region remains approximately constant with temperature, as expected since the 1'-4 alignment should be approximately temperature independent. However, the onset voltage of the positive conductance shifts rapidly to lower biases as the temperature increases, and it is accompanied by an upshift of the whole I-V curve. The upshift of the curves is much intensified at high voltages. This behavior again suggests a leakage channel at high fields, which is consistent with the high activation energy extracted from Fig. 3(b). This leakage already dominates the curve shape at temperatures near $T_{max} \approx 177$ K. For example, see the 172 K curve highlighted by a thick line in Figure 4, in which the NDR is entirely wiped out. This disappearance of NDR is correlated with the sharp increase seen in the threshold current right

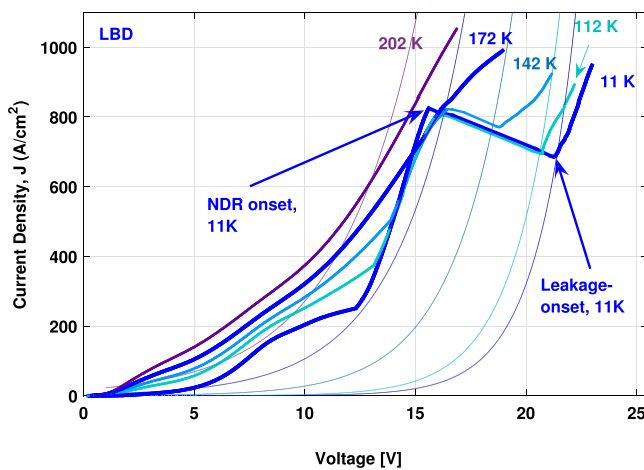


FIG. 4. Current-voltage curves at different temperatures of device LBD (blue scale, solid thick lines) in comparison with simulation of over the barrier current leakage that includes barrier-lowering by the applied voltage (blue scale, thin lines) at the same temperatures of the measurements of device LBD. The measurements at the lowest temperature and at just below T_{max} are highlighted by thicker blue lines. The onset of the NDR and the onset of the current leakage at voltages above it, for the 11 K curve, are marked by blue arrows.

below T_{max} (Figure 3(c)). Together, it suggests that the leakage to the continuum starts dominating the highly diagonal structure near T_{max} , causing a rapid reduction of the upper-state lifetime.

Based on these observations, we postulate that the onset of the positive conductance, for device LBD, is due to thermally activated leakage over the barrier, which increases exponentially with voltage due to the barrier lowering effect (similar to what occurs with dark current in QWIPs⁷). Calculations that include this barrier lowering due to the applied voltage are well correlated with measurements using an escape-barrier height of ~ 140 meV at zero bias (Figure 4). The calculations were conducted according to the simple behavior: $J = J_0 \exp(-\frac{E_b - eV}{k_B T_e})$, where E_b is the zero bias escape-barrier height, eV is the lowering of the barrier by the applied field, and J_0 was estimated with $\sim 30\%$ of the carriers (an approximation for the upper lasing level population), and a characteristic escape time in the continuum of 0.05 ps. The lattice temperatures for the calculation are 10, 110, 140, and 170 K. The excess electronic temperature over the lattice temperature was assumed to be 100 K at zero lattice temperature, and it decreases linearly with temperature to zero at a lattice temperature of 100 K and above.^{2,8} A similar behavior can be shown for carriers escaping the injector level. The temperature behavior of the I-V curves at high biases give further support to our interpretation that the main limiting mechanism (for the highly diagonal structure LBD) is the thermally activated escape of the confined carriers into the continuum.

In conclusion, we suggest that the mechanism responsible for performance degradation at high temperatures, in highly diagonal GaAs/Al_{0.15}GaAs-based THz-QCLs, is the escape of the carriers into the continuum. This process should be significantly reduced in order to improve the temperature performance. It is clear that higher barriers than 15% aluminum concentration will be beneficial to reduce this leakage channel.^{10,11} However, in these earlier works, vertical structures were used in which thermally activated LO-phonon scattering dominate (just like the case for LBD in this work) and these high-barrier structures did not yield a better temperature performance. Going forward, highly diagonal structures based on higher barriers will significantly reduce both the thermally activated LO-phonon scattering and thermal leakage into the continuum. Increasing the aluminum concentration can be done in different ways, as, for example, directly by increasing the ternary composition or alternatively by growing it as digital alloy. Moreover, there is more than one higher-band-offset material system where THz-QCLs have been already demonstrated with reasonable performances and they can serve as platform for improved THz-QCLs with reduced leakage of carriers into the continuum. The “first-choice” In_{0.53}Ga_{0.47}As/Al_{0.48}In_{0.52}As/InP material system is a powerful system for mid-infrared QCLs and have very large conduction band offset of 520 meV. However, in the THz region, the relatively strong coupling demanded by efficient carrier transport requires the growth of very thin Al_{0.48}In_{0.52}As barriers, which makes the laser operation characteristics very sensitive to growth variation and accuracy and limits the laser performances.^{12,13} Lattice

matched $\text{In}_{0.53}\text{Ga}_{0.47}\text{As}/\text{GaAs}_{0.51}\text{Sb}_{0.49}$ THz QCLs in which the $\text{In}_{0.53}\text{Ga}_{0.47}\text{As}$ barriers are replaced by $\text{GaAs}_{0.51}\text{Sb}_{0.49}$ have been recently proposed and demonstrated.^{14,15} This material system enables a smaller band offset (360 meV) together with low barrier effective mass ($0.045m_0$), so thicker barriers can be used.^{14,15} Alternatively, for the same reasons, one can use a quaternary AlInGaAs alloy to replace the thin $\text{Al}_{0.48}\text{In}_{0.52}\text{As}$ barriers.¹³ In such AlInGaAs alloy lattice matched to InP, the effective mass remains smaller than the one of $\text{Al}_{0.48}\text{In}_{0.52}\text{As}$ and the band offset can be tuned from 0 to 520 meV.¹³ The superlattice qualities of these new material systems are still lower than the GaAs/AlGaAs, and further work needs to be done for their improvement.

This research was supported by NSF and Israel MoD. A.A. is partially supported by MIT-Technion and Andrew and Erna Finci Viterbi Fellowships. The authors would like to thank Chun Wang I. Chan for his original measurements, which were used in this work, and to John L. Reno for the MBE growths.

¹U. S. Fatholouloumi, E. Dupont, C. W. I. Chan, Z. R. Wasilewski, S. R. Laframboise, D. Ban, A. Matyas, C. Jirascsek, Q. Hu, and H. C Liu, *Opt. Express* **20**(4), 3866 (2012).

²A. Albo and Q. Hu, *Appl. Phys. Lett.* **106**, 131108 (2015).

³S. Kumar, Q. Hu, and J. L. Reno, *Appl. Phys. Lett.* **94**, 131105 (2009).

⁴G. P. Agrawal and N. K. Dutta, *Long-Wavelength Semiconductor Laser* (Van Nostrand Reinhold Company Inc., Canada, 1986).

⁵J. Faist, *Quantum Cascade Lasers* (Oxford University Press, Great Clarendon Street, Oxford, UK 2013).

⁶J. Faist, C. Sirtori, F. Capasso, A. L. Hutchinson, L. Pfeiffer, and K. W. West, *Opt. Lett.* **21**, 985 (1996).

⁷H. Schneider and H. C. Liu, *Quantum Well Infrared Photodetectors, Physics and Applications* (Springer-Verlag, Berlin, Heidelberg 2007).

⁸C. W. I. Chan, *Towards Room-Temperature Terahertz Quantum Cascade Lasers: Directions and Design* (Massachusetts Institute of Technology, Department of Electrical Engineering and Computer Science, 2015).

⁹S. Kumar, *Development of Terahertz Quantum-Cascade Lasers* (Massachusetts Institute of Technology, Department of Electrical Engineering and Computer Science, 2007).

¹⁰B. S. Williams, S. Kumar, Q. Qin, Q. Hu, and J. L. Reno, *Appl. Phys. Lett.* **88**, 261101 (2006).

¹¹T.-T. Lin, L. Ying, and H. Hirayama, in *Proceedings of the 36th International Conference on Infrared, Millimeter and Terahertz Waves (IRMMW-THz)*, Houston, TX, 2–7 October 2011, pp. 1–2.

¹²M. Fischer, G. Scalari, K. Celebi, M. Amanti, Ch. Walther, M. Beck, and J. Faist, *Appl. Phys. Lett.* **97**, 221114 (2010).

¹³K. Ohtani, M. Beck, G. Scalari, and J. Faist, *Appl. Phys. Lett.* **103**, 041103 (2013).

¹⁴C. Deutsch, A. Benz, H. Detz, P. Klang, M. Nobile, A. M. Andrews, W. Schrenk, T. Kubis, P. Vogl, G. Strasser, and K. Unterrainer, *Appl. Phys. Lett.* **97**, 261110 (2010).

¹⁵C. Deutsch, M. Krall, M. Brandstetter, H. Detz, A. M. Andrews, P. Klang, W. Schrenk, G. Strasser, and K. Unterrainer, *Appl. Phys. Lett.* **101**, 211117 (2012).